Shortening Solitons for Fiber-Optic Transmission

Wahls, S.

DOI
10.1109/ISWCS49558.2021.9562241

Publication date
2021

Document Version
Accepted author manuscript

Published in
Proceedings of the 17th International Symposium on Wireless Communication Systems (ISWCS 2021)

Shortening Solitons for Fiber-Optic Transmission

Sander Wahls
Delft Center for Systems and Control, Delft University of Technology, The Netherlands. Email: s.wahls@tudelft.nl.

***Abstract*—Solitons are stable localized pulses that do not disperse in optical fiber. When several solitons interact, they form a multi-soliton. Various fiber-optic communication systems based on multi-solitons have been investigated, but their spectral efficiencies are not competitive. One issue with using multi-solitons for communications is that their effective duration can vary widely with the number of interacting solitons. In this paper, we therefore introduce the concept of soliton shortening. In soliton shortening, a dispersive part is added to the nonlinear spectrum of a multi-soliton that reduces the pulse to a fixed finite duration, *without changing the characteristics of the solitonic part*. As a proof of concept, soliton shortening is shown to increase the spectral efficiency of a 2-soliton on-off keying system by 40%.**

I. Introduction

The fiber-optic channel is inherently nonlinear due to the Kerr effect [1]. Many fiber-optic communication systems are designed to avoid this issue, and operate in regimes where nonlinear effects are weak. However, there are also attempts to embrace the nonlinearity instead of avoiding it. Solitons are stable localized pulses that do not disperse during propagation due to the Kerr effect. This makes them interesting for information transmission, and in the past many soliton communication systems have been investigated [2]. In these early systems, trains of single solitons were typically generated optically. With the advent of coherent receivers and digital signal processing, it has become possible to go beyond single solitons. The nonlinear Fourier transform (NFT) decomposes a signal into solitonic and dispersive components [3,4]. In an ideal (i.e., loss- and noise-free) nonlinear fiber, the evolution of these components is decoupled from each other and can be described using simple analytic formulas. The inverse NFT conversely synthesizes signals with prescribed solitonic and dispersive parts. In the last ten years, many different fiber-optic communication systems based on NFTs have been proposed. See, e.g., [4,5]. In most designs, either the solitonic part or the dispersive part of the NFT is used exclusively. There are a few works in which small numbers of solitons are added to a dispersive part [6]–[9], but the amount of energy in the solitonic part is small. Interestingly, one can observe a different picture when the NFT of conventionally modulated signals is taken. At higher powers, solitons carry most of the energy and the dispersive part plays a minor role [10]–[12]. On the other hand, it was found that the energy contained in a directly modulated dispersive part can be bounded [13].

Instead of adding carefully chosen solitons to a given dispersive part, in this paper we add a carefully designed dispersive part to a given multi-soliton such that its fitness for data transmission is improved. We develop a new approach called *soliton shortening* to achieve this goal. Specifically, soliton shortening turns a multi-soliton, which decays quickly but has infinite duration, into a finite duration signal *without changing the solitonic part of the NFT*. As a proof of concept, we use soliton shortening to harmonize the pulse durations for a two-soliton on-off keying (OOK) transceiver (see, e.g., [14]), which leads to an increase in spectral efficiency of 40%.

The paper is structured as follows. Sec. II recalls some known results, mostly regarding the fiber-optic channel and the NFT. Then, two soliton shortening methods are presented in Sec. III. In Sec. IV, soliton shortening is used to improve a two-soliton OOK system. The paper is concluded in Sec. V.

This project has received funding from the European Research Council (ERC) under the European Union's Horizon 2020 Research and Innovation Programme (grant agreement No 716669).

II. Preliminaries

A. Channel Model

The fiber-optic communication channel is modeled by the nonlinear Schrödinger equation (NSE) [1, Eq. 7.1.4]

$$\frac{\partial A}{\partial \mathsf{z}} + j\frac{\beta_2}{2}\frac{\partial^2 A}{\partial \mathsf{t}^2} = j\gamma|A|^2 + \frac{1}{2}[g_0 - \alpha]A + f, \qquad (1)$$

where j is the imaginary number, and $A(\mathsf{z},\mathsf{t})$ represents the electromagnetic field at location z [m] and time t [s]; the squared brackets indicate SI units. The unit of $|A|$ is $\sqrt{\mathrm{W}}$. The coefficients α [m^{-1}], β_2 [$\mathrm{s}^2\mathrm{m}^{-1}$] and γ [$\mathrm{W}^{-1}\mathrm{m}^{-1}$] characterize the loss, dispersion and Kerr nonlinearity of the fiber, respectively. The profile $g_0(\mathsf{z})$ depends on the amplification scheme. Ideal distributed Raman amplification corresponds to $g_0(\mathsf{z}) = \alpha$, while lumped EDFA amplification corresponds to $g_0(\mathsf{z}) = G\sum_{n=1}^{\infty}\delta(\mathsf{z} - nS)$ with G [] being a gain and S [m] being the amplifier spacing. The term $f(\mathsf{z},\mathsf{t})$ finally represents noise. In the context of NFTs, it is convenient to neglect noise and normalize the NSE. For anomalous dispersion fiber, the normalized field $q(z,t)$ obeys

$$j\frac{\partial q}{\partial z} + \frac{1}{2}\frac{\partial^2 q}{\partial t^2} + |q|^2 q = 0, \quad q = q(z,t), \qquad (2)$$

where z and t are normalized versions of the location z and time t. The precise normalization depends on the amplification scheme. With ideal distributed amplification, the normalized NSE (2) is equivalent to (1) (in the absence of noise). When the dispersion and nonlinearity coefficients are allowed to vary in space, then the normalization can also be exact for lumped amplification [15]. In this paper, we use the normalization from [16] for the constant coefficient case. The normalized NSE (2) only approximates the original NSE (1) in this case.

B. Nonlinear Fourier Transform (NFT)

The NFT of the time-domain signal $q(z_0,t)$ is defined with the help of the Zakharov-Shabat scattering problem [3]

$$\frac{d\boldsymbol{\phi}}{dt} = \begin{bmatrix} -j\lambda & q \\ -q^* & j\lambda \end{bmatrix} \boldsymbol{\phi}, \quad \lim_{t\to-\infty} e^{j\lambda t}\boldsymbol{\phi} = \begin{bmatrix} 1 \\ 0 \end{bmatrix},$$

$$\boldsymbol{\phi} = \boldsymbol{\phi}(z_0,t,\lambda) = \begin{bmatrix} \phi_1(z_0,t,\lambda) \\ \phi_2(z_0,t,\lambda) \end{bmatrix}, \; q(z_0,t) \overset{|t|\to\infty}{\longrightarrow} 0 \text{ "fast".}$$

Here, the asterisk * denotes the complex conjugate. The scattering coefficients of $q(z_0,t)$ are given by $a(\lambda) = a(z_0,\lambda) := \lim_{t\to\infty} e^{j\lambda t}\phi_1(z_0,t,\lambda)$ and $b(\lambda) = b(z_0,\lambda) := \lim_{t\to\infty} e^{-j\lambda t}\phi_2(z_0,t,\lambda)$. They always satisfy the relation

$$a(\xi)a^*(\xi^*) + b(\xi)b^*(\xi^*) = 1, \quad \forall \xi \in \mathbb{R}. \tag{3}$$

The NFT of $q(z_0,t)$ consists of a continuous spectrum $b(\xi)$, $\xi \in \mathbb{R}$, and a finite discrete spectrum (λ_n, b_n), $n = 1,\dots,N$, where the so-called eigenvalues λ_n are the solutions of $a(\lambda) = 0$ with imaginary part $\Im(\lambda) > 0$; the b_n are called norming constants. The continuous spectrum represents dispersive components of q, while the discrete spectrum indicates solitonic components.

If $q(z,t)$ is a solution of the normalized NSE (2), then the scattering coefficients evolve in a very simple manner:

$$a(z,\lambda) = a(0,\lambda), \quad b(z,\lambda) = e^{2j\lambda^2 z} b(0,\lambda). \tag{4}$$

Therefore, we know exactly how the NFT of a pulse launched at $z = 0$ evolves when it propagates according to the NSE (2).

C. Nonlinear Fourier Transform of Time-Limited Signals

Early NFT-based fiber-optic transmission systems used a different definition of the NFT that made it difficult to control the temporal support of pulses generated by modulation of the continuous part of the NFT. In [17], it was recognized that these problems can be avoided by using the definition of the NFT above. The NFT of a time-limited signal $q(z_0,t)$, i.e.

$$q(z_0,t) = 0, \quad \forall |t| > T, \tag{5}$$

has a band-limited continuous part. More precisely, the Fourier transform of the b-coefficient of a time-limited signal satisfies

$$\mathcal{F}[b](\tau) := \int_{-\infty}^{\infty} b(\xi) e^{-j\xi\tau} d\xi = 0, \; \forall |\tau| > 2T. \tag{6}$$

This implies that $b(\lambda)$ is an entire function. Thus, (3) extends into the complex plane, and the discrete spectrum satisfies

$$b(\lambda_n)b^*(\lambda_n^*) = 1, \quad b_n = b(\lambda_n), \quad \forall n = 1,\dots,N. \tag{7}$$

These conditions are also sufficient [18]. To give a precise statement, we require the Paley-Wiener space $\mathcal{PW}_\sigma^1$.

Definition 1. We denote the space of Lebesgue integrable complex-valued functions on $\mathbb{R}$ by $\mathcal{L}^1$. The Paley-Wiener space $\mathcal{PW}_\sigma^1$ contains all functions of the form

$$f(\lambda) = \frac{1}{2\pi}\int_{-\sigma}^{\sigma} F(\tau) e^{j\lambda\tau} d\tau, \quad F \in \mathcal{L}^1, \quad \lambda \in \mathbb{C}.$$

(Note that functions in $\mathcal{PW}_\sigma^1$ are entire and therefore already uniquely specified their values on the real line.)

Theorem 6 in [18] ensures that for any $b(z_0,\cdot) \in \mathcal{PW}_{2T}^1$ with $|b(z_0,\xi)| < 1$ for all $\xi \in \mathbb{R}$, and any discrete spectrum (λ_n, b_n) that satisfies (7), there is exactly one signal $q(z_0,\cdot) \in \mathcal{L}^1$ with this nonlinear spectrum. This signal satisfies (5).

D. 99%-Duration and Bandwidth

For any $g : \mathbb{R} \to \mathbb{C}$, we set $E_I(g) := \int_{-I/2}^{I/2} |g(s)|^2 ds$. Then the 99%-duration and bandwidth of $q(t) = q(z_0,t)$ are

$$D_{99\%}(q) := \min\{D > 0 : E_D(q) \geq 0.99 E_\infty(q)\},$$
$$B_{99\%}(q) := \min\{B > 0 : E_{2\pi B}(Q) \geq 0.99 E_\infty(Q)\},$$

where $Q := \mathcal{F}[q]$ is the conventional Fourier transform of $q(t)$.

III. Soliton Shortening

Multi-solitons are signals for which the discrete part of the nonlinear spectrum is non-empty, while the continuous part is trivial in the sense that the b-coefficient is identical to zero, $b(\xi) = 0$ for all $\xi \in \mathbb{R}$. The real and imaginary parts of the eigenvalues λ_n indicate the speed and amplitude of each solitonic component, while the norming constants b_n are related to their phases. The temporal support of multi-solitons in communication systems can vary widely, which typically reduces the spectral efficiency of the overall system. We are thus interested in using the normally unused continuous part of the nonlinear spectrum of a multi-soliton to shorten the corresponding time-domain signal to a finite, given duration. We had seen in Sec. II-C that the discrete and continuous parts of the NFT are coupled for time-limited signals. In light of these constraints, our formal problem statement is as follows.

Problem 2 (Soliton Shortening)**.** Given a desired duration $T > 0$ and a desired discrete spectrum (λ_n, b_n) such that

$$\Im(\lambda_n) > 0 \text{ and } m \neq n \Rightarrow \lambda_m \neq \lambda_n, \quad \forall m,n = 1,\dots,N,$$

find a continuous spectrum $b \in \mathcal{PW}_{2T}^1$ such that

1) $b(\lambda_n)b^*(\lambda_n^*) = 1$ for all $n = 1,\dots,N$,
2) $b(\lambda_n) = b_n$ for all $n = 1,\dots,N$, and
3) $|b(\xi)| < 1$ for all $\xi \in \mathbb{R}$.

Given a solution to the soliton shortening problem, we can use an inverse NFT to construct a time-limited signal as in (5) that has the desired discrete spectrum (λ_n, b_n).

In the following, we present two methods for finding solution candidates $b \in \mathcal{PW}_{2T}^1$ for Problem 2 that fulfill the first two conditions. The third condition may or may not be fulfilled. If it is, we found a solution to the soliton shortening problem. Otherwise, we have to try different parameters.

A. Method A

Method A is based on Lagrange interpolation. We define

$$\lambda_{N+n} := \lambda_n^*, \quad b_{N+n} := \frac{1}{b_n^*}, \quad n = 1,\dots,N,$$

and choose our first solution candidate for Problem 2 as

$$b(\lambda) = \sum_{m=1}^{2N} b_m L_m(\lambda),$$

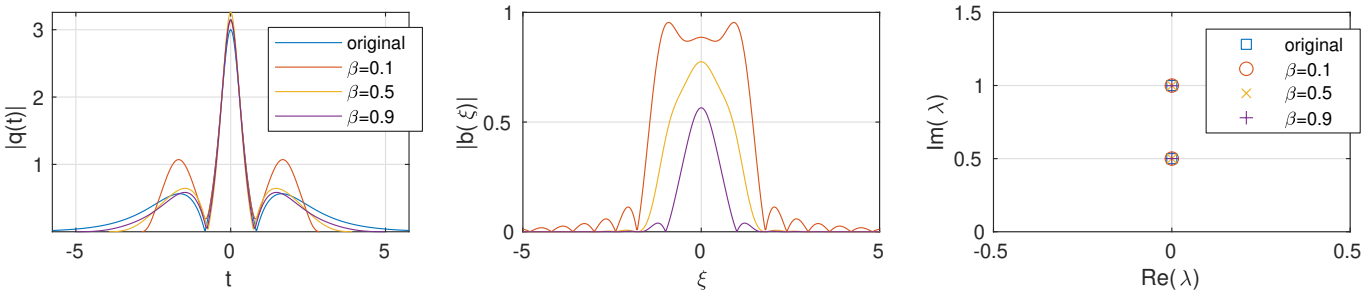

(a) Method A with $\mathcal{T} = 0.6$, $\zeta_1 = \mathcal{T}$, $\zeta_2 = 2\mathcal{T}$, $\zeta_3 = -\zeta_1$, and $\zeta_4 = -\zeta_2$.

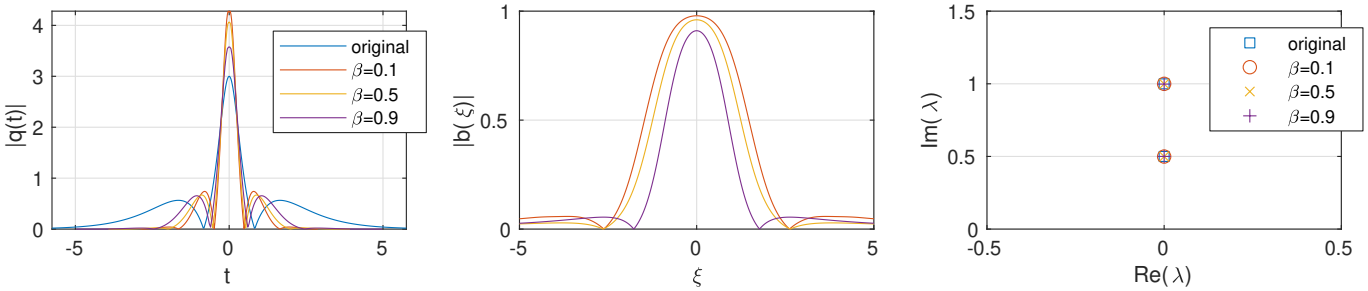

(b) Method B with $\mathcal{T} = 0.6$, $r = 64$, $\zeta_2 = -\zeta_1$, $\zeta_3 = \zeta_1^*$, and $\zeta_4 = \zeta_2^*$. The value of ζ_1 is $1.33881189472387 + 1.26256436322092j$ for $\beta = 0.1$, $1.06596632148789 + 1.15763272061821j$ for $\beta = 0.5$, and $0.840263882796328 + 0.969670479860097j$ for $\beta = 0.9$.

Figure 1: Comparison of the Methods A and B for $N = 2$, $\lambda_n = \frac{n}{2}j$ and $b_n = 1$. The shortened $q(t)$ are zero for $|t| > T = \pi\frac{1+\beta}{2\mathcal{T}}$.

where the (still to be specified) functions $L_n(\lambda)$ satisfy

$$m \neq n \;\Rightarrow\; L_m(\lambda_n) = 0, \quad L_n(\lambda_n) = 1. \tag{8}$$

The first two conditions in Problem 2 are then fulfilled since

$$b(\lambda_n) = \sum_{m=1}^{2N} b_m L_m(\lambda) = b_n \underbrace{L_n(\lambda_n)}_{=1} + \sum_{\substack{m=1\\m\neq n}}^{2N} b_m \underbrace{L_m(\lambda_n)}_{=0}$$

$$\Rightarrow\; b(\lambda_n)b^*(\lambda_n^*) = b(\lambda_n)b^*(\lambda_{N+n}) = b_n b_{N+n}^* = \frac{b_n}{b_n^{**}} = 1$$

for all $n = 1, \ldots, N$. We only need to choose suitable interpolation basis functions $L_1, \ldots, L_{2N}$. The problem here is that classical Lagrange polynomials are not in $\mathcal{PW}_{2T}^1$ as required in Problem 2. We therefore instead use

$$L_n(\lambda) := \frac{\psi(\lambda)R_n(\lambda)}{\psi(\lambda_n)R_n(\lambda_n)}, \quad R_n(\lambda) := \prod_{\substack{m=1\\m\neq n}}^{2N} \frac{1-\lambda/\lambda_m}{1-\lambda/\zeta_m}, \tag{9}$$

where ψ denotes the impulse response of a raised cosine filter:

$$\psi(\lambda) = \begin{cases} \frac{\pi}{4\mathcal{T}}\operatorname{sinc}\left(\frac{1}{2\beta}\right) & , \lambda = \pm\frac{\mathcal{T}}{2\beta} \\ \frac{1}{\mathcal{T}}\operatorname{sinc}\left(\frac{\lambda}{\mathcal{T}}\right)\frac{\cos\left(\frac{\pi\beta\lambda}{\mathcal{T}}\right)}{1-\left(\frac{2\beta\lambda}{\mathcal{T}}\right)^2} & , \lambda \neq \pm\frac{\mathcal{T}}{2\beta} \end{cases}. \tag{10}$$

Here $\mathcal{T} > 0$ and $\beta \in (0, 1]$ are free parameters, $\operatorname{sinc}(\lambda) = \frac{\sin\pi\lambda}{\pi\lambda}$ for $\lambda \neq 0$ and $\operatorname{sinc}(0) = 1$. The ζ_n in (9) are furthermore arbitrarily chosen pairwise different zeros of $\psi(\lambda)$, i.e.,

$$\{\zeta_1, \ldots, \zeta_{2N}\} \subset \{\pm\mathcal{T}, \pm 2\mathcal{T}, \cdots\}, \quad m \neq n \Rightarrow \zeta_m \neq \zeta_n.$$

Direct substitution shows that the functions (9) satisfy the interpolation condition (8). Furthermore, it is known that

$$\psi \in \mathcal{PW}_{\pi(1+\beta)/\mathcal{T}}^1. \tag{11}$$

Note that the rational product in (9) moves $2N-2$ zeros of ψ to new locations. It is known that this operation does not change the band-limitation [19, IV.D]. (In fact, L_n is a slightly generalized version of [20, Eq. 5].) Since the poles of the rational product R_n are cancelled by zeros of ψ and R_n is furthermore proper, $L_n \in \mathcal{L}^1$. This implies $\mathcal{F}[L_n] \in \mathcal{L}^\infty$. Since L_n is also band-limited, we find that $\mathcal{F}[L_n] \in \mathcal{L}^1$. Hence,

$$L_n \in \mathcal{PW}_{\pi(1+\beta)/\mathcal{T}}^1,\ \forall n \quad \Rightarrow \quad b \in \mathcal{PW}_{\pi(1+\beta)/\mathcal{T}}^1.$$

We therefore found a candidate solution for Problem 2 if we choose the parameters β and $\mathcal{T}$ such that $2T = \pi\frac{1+\beta}{\mathcal{T}}$. If the constructed $b(\lambda)$ in addition satisfies $|b(\xi)| < 1$ for all $\xi \in \mathbb{R}$, then it is a solution. If not, then we have to try again with different parameters, as was already mentioned before.

B. Method B

Our second solution candidate for Problem 2 is

$$b(\lambda) := \pm 1 - f(\lambda)R(\lambda), \quad R(\lambda) := \prod_{m=1}^{2N} \frac{\lambda - \lambda_m}{\lambda - \zeta_m}, \tag{12}$$

where $f(\lambda) := 1 - \frac{1}{r}\psi(\lambda)$ with $r > 0$, the ± 1 is a parameter, $\psi(\lambda)$ is still given by (10), and $\lambda_{N+n} := \lambda_n^*$ for $n = 1, \ldots, N$. The $\zeta_1, \ldots, \zeta_{2N}$ are now (numerically found) non-real zeros of f. We assume that the following two conditions are fulfilled,

$$\sum_{m=1}^{2N} (\zeta_m - \lambda_m) = 0 \quad \text{and} \quad m \neq n \Rightarrow \zeta_m \neq \zeta_n. \tag{13}$$

We now discuss the conditions from Problem 2. Note that

$$b(\lambda_n) = \pm 1 - f(\lambda_n)R(\lambda_n) = \pm 1 - f(\lambda_n)0 = \pm 1,$$
$$b^*(\lambda_n^*) = b^*(\lambda_{N+n}) = \pm 1^* - f^*(\lambda_{N+n})0 = \pm 1.$$

The first condition in Problem 2 is thus always fulfilled, while the second condition is fulfilled if and only if

$$b_1 = \cdots = b_N = \pm 1. \tag{14}$$

We still need to investigate if (12) is in $\mathcal{PW}^1_{2T}$. Since the Fourier transform of $\lambda \mapsto 1$ is a Dirac delta at $\tau = 0$, we find that $f(\lambda) = 1 + \frac{1}{r}\psi(\lambda)$ is still band-limited with $\mathcal{F}[f](\tau) = 0$ for $|\tau| > \pi\frac{1+\beta}{\mathcal{T}}$. However, $\mathcal{F}[f]$ is not in $\mathcal{L}^1$, and hence also not in $\mathcal{PW}^1_{\pi(1+\beta)/\mathcal{T}}$, due to the delta pulse. The multiplication of f with R in (12) again moves $2N$ zeros of f. Even though the result in [19, IV.D] only states that moving zeros keeps the band-limit intact for finite energy signals, numerical tests indicate that this still works in our case here. *Assuming that this is indeed true*, we find that $\mathcal{F}[fR](\tau) = 0$, and thus

$$\mathcal{F}[b](\tau) = \mathcal{F}[\pm 1 - fR](\tau) = 0, \text{ for } |\tau| > \pi\frac{1+\beta}{\mathcal{T}}. \tag{15}$$

Furthermore, note that

$$b = 1 - (1 - r^{-1}\psi)R = 1 - R + r^{-1}\psi R.$$

The function $1-R$ is strictly proper rational without poles on $\mathbb{R}$. Since $1-R \approx \lambda^{2N-1}\sum_{m=1}^{2N}(\lambda_m - \zeta_m)\Big/\lambda^{2N}$ for $|\lambda|$ large, (13) ensures that $1-R$ has a non-simple zero at infinity. Thus, $1-R \in \mathcal{L}^1$. Similarly, R is proper without poles on $\mathbb{R}$ and therefore bounded. Since $\psi \in \mathcal{L}^1$, this implies $r^{-1}\psi R \in \mathcal{L}^1$ and thus $b \in \mathcal{L}^1$. This in turn implies that $\mathcal{F}[b]$ is in $\mathcal{L}^\infty$ (and thus bounded), which together with (15) finally shows that $\mathcal{F}[b] \in \mathcal{L}^1$. Assuming that (15) is indeed true, this finally implies $b \in \mathcal{PW}^1_{\pi(1+\beta)/\mathcal{T}}$. We therefore found another candidate solution for Problem 2 if we choose β and $\mathcal{T}$ s.t. $2T = \pi\frac{1+\beta}{\mathcal{T}}$. Due to (14), *all b_n have to be equal (either 1 or -1) for this method.*

C. Numerical Example

We now compare both methods in a numerical example. The multi-soliton that will be shortened is shown as a blue curve in the left plot in Fig. 1a. Its nonlinear spectrum is purely discrete with $\lambda_n = \frac{n}{2}j$, $b_n = 1$, $n = 1, 2$. The multi-soliton decays exponentially fast, but it is of infinite duration. The other curves in the left plot in Fig. 1a show the shortened signals for Method A for different values of the parameters β, which controls the shape of the raised cosine impulse response (10). The other parameters were fixed and can be found in the caption of Fig. 1a. The support $[-T, T]$ of the generated finite duration signal (5) varies since $2T = \pi(1+\beta)/\mathcal{T}$. The center plot in Fig. 1a illustrates the corresponding b-coefficients. We can see that the more the multi-soliton is shortened, the stronger the added continuous spectrum becomes. In this example, all $b(\xi)$ generated by Method A still fulfill the third condition in Prob. 2, but for larger values of $\mathcal{T}$ that is no longer the case. The right plot in Fig. 1a finally shows the numerically computed eigenvalues for each of the signals. It confirms that the eigenvalues of the shortened signals indeed coincide with the eigenvalues of the original multi-soliton as desired. The norming constants (not shown) match as well. Fig. 1b shows analog plots for Method B. We find that also Method B successfully shortens the multi-soliton in all cases.

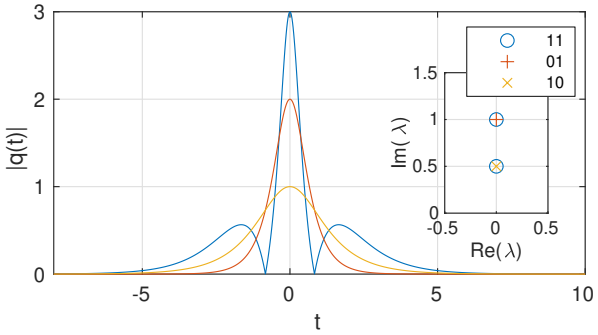

Figure 2: Illustration of soliton on-off keying for the eigenvalue locations $\lambda = 0.5j$ and $\lambda = 1j$. The large plot shows the time domain signals that correspond to the discrete spectra in the smaller plot. The norming constants (not shown) were all one. The 00 signal is identical zero and therefore not shown.

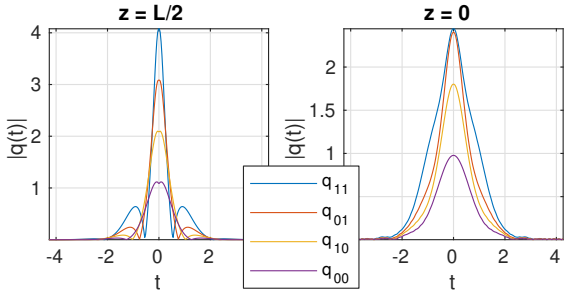

(a) Shortened. Note that $q_{00}(t) \not\equiv 0$ since $b(\lambda) = \text{Eq. } 12 \not\equiv 0$.

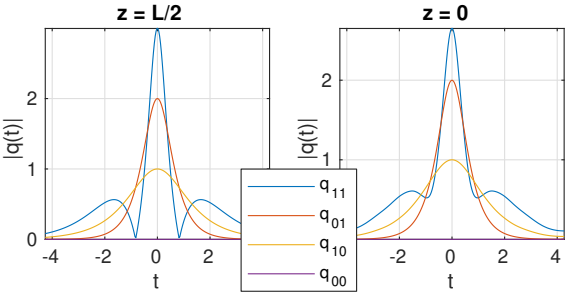

(b) Original.

Figure 3: Illustration of the two transmit alphabets.

The durations of the shortened signals are the same for both methods when β and $\mathcal{T}$ coincide, but the signals generated by Method B are more concentrated around the center at $t = 0$. Thus, Method B generates "effectively shorter" signals than Method A in this example. However, we emphasize again that Method B only applies if all norming constants are either 1 or -1. Therefore, it is less flexible than Method A.

IV. Improved Solitonic On-Off Keying

We now discuss an application of soliton shortening. Soltion on-off keying (OOK) is a communication technique in which a bit is signaled through the presence or absence of an eigenvalue at a prescribed position. Fig. 2 shows the transmit signals generated by an exemplary two-bit soliton OOK transmitter.

α	$\frac{1}{10}\log(10)\times 0.2\times 10^{-3}$ m^{-1}
β_2	-21.5×10^{-27} s^{2}m^{-1}
γ	10^{-3} W^{-1}m^{-1}
T_0	2.0317×10^{-10} s
Span length	80 km
Link length	960 km
Noise figure	5 dB

Table I: Simulation parameters

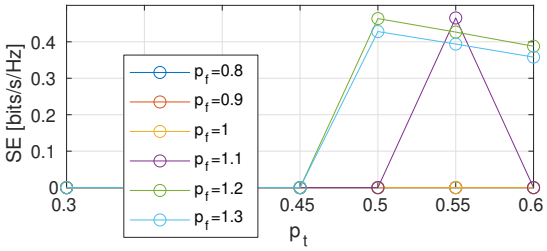

(a) Shortened

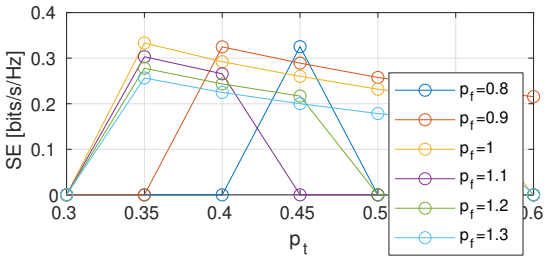

(b) Original

Figure 4: Spectral efficiencies

The appeal of soliton OOK is that *a)* (multi-)solitons do not disperse during propagation, and *b)* the eigenvalues are easily localized at the receiver since they stay constant during propagation in an ideal fiber [due to (4)]. The principle was explored in various papers [4,14,21]–[23], but in general the interest in soliton OOK has been low since the achieved spectral efficiencies were much lower than for other NFT-based techniques. The problem is that the effective durations (and also bandwidths) of the different pulses in a soliton OOK system vary widely. Some of the signals are long (and have a relatively low bandwidth), while others are short (and have a higher bandwidth). This can already be seen for the simple two eigenvalue case in Fig. 2. The maximum duration and the maximum bandwidth that the transmitter and receiver have to accommodate are therefore both high. Hence, the system occupates a large area in the time-frequency plane, resulting in low overall spectral efficiencies.

In this section, we will show that soliton shortening can be used to alleviate this problem and improve the spectral efficiency of soliton OOK systems. Specifically, we will use Method B from in Sec. III-B to improve the spectral efficiency of the soliton OOK system illustrated in Fig. 2.

A. Simulation Setup

In our simulations, we considered a 12×80km standard single-mode fiber link with lumped amplification with most parameters as in [24]. The simulation parameters are summarized in Tab. I. The simulation included ideal low-pass filters at the transmitter and receiver to account for band-width constraints during D/A and A/D conversion, and was realized using components from the current development version (commit `a7cd9d2`) of NFDMLab [25]. In each simulation, 5000 signals were randomly drawn from an alphabet of transmit signals. Each of the drawn signals was then truncated to a fixed interval $[-D_{\text{eff}}/2, D_{\text{eff}}/2]$. The truncated signals were concatenated, and the resulting signal train was low-pass filtered with cut-off frequency $B_{\text{eff}}/2$. The filtered signal train was propagated and filtered again (with the same cut-off) at the receiver. There, the signal train was cut and the NFTs of the individual received signals were computed using FNFT [26]. Finally, bit error rates (BERs) were computed. No coding was applied. Since we transmitted two bits per signal (i.e., 10000 bits per simulation), the spectral efficiency of the system was estimated as

$$\text{SE} = \begin{cases} \frac{2}{D_{\text{eff}}B_{\text{eff}}}, & \text{BER} \leq 10^{-3} \\ 0, & \text{otherwise} \end{cases} \left[\frac{\text{bits}}{\text{s}\times\text{Hz}}\right]. \tag{16}$$

Two different alphabets of transmit signals were used in the simulations. Both were derived from the transmitter in Fig. 2. For the first alphabet, the signals were first shortened using Method B with parameters $\beta = 0.9$, $\mathcal{T} = 0.7$, $r = 64$ and

$$\zeta_{1,2} = \pm 0.976549665010138 + 1.15273776148887j.$$

To compensate for the spreading of the dispersive part that was added to shorten the signals, the shortened signals were then back-propagated to $z = -L/2$, where L is the normalized propagation distance. The second alphabet contained the back-propagated versions of the original two-soliton OOK transmitter (even as these do not disperse). The alphabets are illustrated in Fig. 3. The left plots ($z = L/2$) show the signals after ideal propagation through the first half of the fiber link. Since this compensates the initial back-propagation, these signals are identical to the initial (shortened or original) multi-solitons. The right plots ($z = 0$) show the corresponding back-propagated signals, i.e., the actual transmit alphabets.

B. Simulation Results

It turned out that the transmit signals could be truncated and/or low-pass filtered further without noticeable performance impairments. To find the best configuration, the effective duration D_{eff} and bandwidth B_{eff} used by the transmitter to truncate and respectively filter the signals before transmission (see Sec. IV-A) were swept as follows. Recall the 99%-duration and bandwidth defined in Section II-D. We denote their maxima taken over all signals in a signal alphabet by

$$D_{99\%}^{\max} := \max_q D_{99\%}(q) \quad \text{and} \quad B_{99\%}^{\max} := \max_q B_{99\%}(q).$$

The spectral efficiency (16) of each of the two transmit alphabets was determined in individual simulations for

$$D_{\text{eff}} = p_t D_{99\%}^{\max}, \quad B_{\text{eff}} = p_f B_{99\%}^{\max}$$

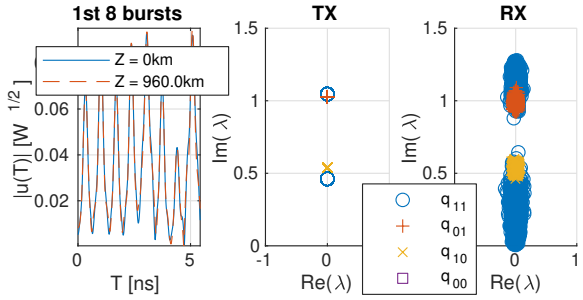

(a) Shortened

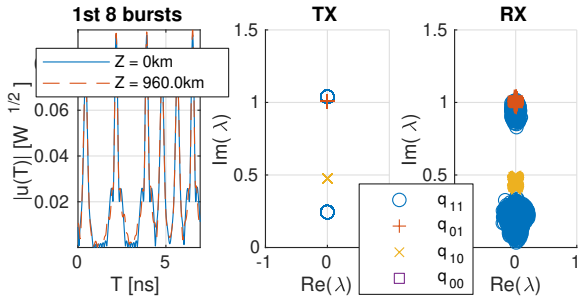

(b) Original

Figure 5: Time domain and constellations at maximal SE

with $p_t \in \{0.3, 0.35, \ldots, 0.6\}$ and $p_f \in \{0.8, 0.9, \ldots, 1.3\}$. The results are shown in Fig. 4. The peak efficiency of the shortened two-soliton OOK transmitter is 0.4655 bits/s/Hz. This is an improvement of 40% over the original two-soliton OOK transmitter, whose peak efficiency is 0.3333 bits/s/Hz. Fig. 5 depicts time domain signals and constellations for both transmitters at maximum efficiency. Note that the optimally truncated shortened transmit alphabet still contains shorter signals than the optimally truncated original transmit alphabet.

V. Conclusion

We introduced the concept of soliton shortening, which means that a multi-soliton is turned into a finite duration signal without harming the discrete spectrum; the desired duration is a free parameter. Two different soliton shortening methods were presented. One of these methods was used to improve the spectral efficiency of a two-soliton on-off keying system. There are various interesting questions for future research. From a theoretical point of view, it would be interesting to know under which circumstances a multi-soliton can be shortened to a given duration. The methods presented in this paper have disadvantages. Method A applies to arbitrary discrete spectra but may fail in cases where Method B succeeds, while Method B applies only to specific norming constants. An improved method that combines the flexibility of Method A with the stronger shortening capabilities of Method B would be of interest. Finally, the application of soliton shortening to more involved communication systems should be investigated.

References

[1] G. P. Agarwal, *Fiber-Optic Communication Systems*. Wiley, 2010.

[2] A. Hasegawa and M. Matsumoto, *Optical Solitons in Fibers*. Springer, 2003.

[3] V. F. Zakharov and A. B. Shabat, "Exact theory of two-dimensional self-focusing and one-dimensional self-modulation of waves in nonlinear media," *Sov. Phys. JETP*, vol. 34, p. 62–69, Jan. 1972.

[4] M. I. Yousefi and F. R. Kschischang, "Information transmission using the nonlinear Fourier transform, Parts I–III," *IEEE Trans. Inf. Theory*, vol. 60, p. 4312–4369, July 2014.

[5] S. K. Turitsyn, J. E. Prilepsky, S. T. Le, S. Wahls, L. L. Frumin, M. Kamalian, and S. A. Derevyanko, "Nonlinear Fourier transform for optical data processing and transmission: Advances and perspectives," *Optica*, vol. 4, no. 3, p. 307–322, 2017.

[6] S. T. Le, V. Aref, and H. Buelow, "Nonlinear signal multiplexing for communication beyond the Kerr nonlinearity limit," *Nature Photonics*, vol. 11, no. 9, p. 570–576, 2017.

[7] A. Vasylchenkova, J. E. Prylepsky, N. B. Chichkov, and S. K. Turitsyn, "Multieigenvalue communication paired with b-modulation," in *Proc. Europ. Conf. Optical Commun. (ECOC)*, p. 1–4, 2019.

[8] A. Vasylchenkova, J. E. Prilepsky, N. B. Chichkov, and S. K. Turitsyn, "Combining the discrete NFT spectrum with b-modulation for high-efficiency optical transmission," in *Proc. Conf. Lasers Electro-Optics Europe and Europ. Quantum Electron. Conf.*, p. ci_2_5, 2019.

[9] B. Leible, D. Plabst, and N. Hanik, "Back-to-back performance of the full spectrum nonlinear Fourier transform and its inverse," *Entropy*, vol. 22, no. 10, 2020.

[10] S. Wahls, S. T. Le, J. E. Prilepsky, H. V. Poor, and S. K. Turitsyn, "Digital backpropagation in the nonlinear Fourier domain," in *Proc. IEEE Wksp. Adv. Signal Process. Adv. Wireless Commun. (SPAWC)*, (Stockholm, Sweden), p. 445–449, June 2015.

[11] S. Turitsyn, E. Sedov, A. Redyuk, and M. Fedoruk, "Nonlinear spectrum of conventional OFDM and WDM return-to-zero signals in nonlinear channel," *IEEE/OSA J. Lightwave Technol.*, vol. 38, p. 352–358, 2020.

[12] P. de Koster and S. Wahls, "Dispersion and nonlinearity identification for single-mode fibers using the nonlinear Fourier transform," *IEEE/OSA J. Lightwave Technol.*, vol. 38, no. 12, p. 3252–3260, 2020.

[13] S. Chimmalgi and S. Wahls, "Bounds on the transmit power of b-modulated NFDM systems in anomalous dispersion fiber," *Entropy*, vol. 22, no. 6, 2020.

[14] S. Hari, M. I. Yousefi, and F. R. Kschischang, "Multieigenvalue communication," *J. Lightwave Technol.*, vol. 34, p. 3110–3117, 2016.

[15] V. Bajaj, S. Chimmalgi, V. Aref, and S. Wahls, "Exact NFDM transmission in the presence of fiber-loss," *IEEE/OSA J. Lightwave Technol.*, vol. 38, no. 11, p. 3051–3058, 2020.

[16] S. T. Le, J. E. Prilepsky, and S. K. Turitsyn, "Nonlinear inverse synthesis technique for optical links with lumped amplification," *Opt. Express*, vol. 23, p. 8317–8328, Apr 2015.

[17] S. Wahls, "Generation of time-limited signals in the nonlinear Fourier domain via b-modulation," in *Proc. European Conference on Optical Communication (ECOC)*, p. 1–3, 2017.

[18] D. Shepelsky, A. Vasylchenkova, J. E. Prilepsky, and I. Karpenko, "Nonlinear Fourier spectrum characterization of time-limited signals," *IEEE Trans. Commun.*, vol. 68, no. 5, p. 3024–3032, 2020.

[19] A. A. G. Requicha, "The zeros of entire functions: Theory and engineering applications," *Proc. IEEE*, vol. 68, no. 3, p. 308–328, 1980.

[20] F. Bond and C. Cahn, "On sampling the zeros of bandwidth limited signals," *IRE Trans. Inf. Theor.*, vol. 4, no. 3, p. 110–113, 1958.

[21] Z. Dong, S. Hari, T. Gui, K. Zhong, M. I. Yousefi, C. Lu, P.-K. Wai, F. Kschischang, and A. Lau, "Nonlinear frequency division multiplexed transmissions based on NFT," *IEEE Photonics Lett.*, vol. 27, no. 15, p. 1621–1623, 2015.

[22] V. Aref, Z. Dong, and H. Buelow, "Design aspects of multi-soliton pulses for optical fiber transmission," in *IEEE Photonics Conf (IPC)*, 2016.

[23] B. Leible, Y. Chen, M. I. Yousefi, and N. Hanik, "Soliton transmission with 5 eigenvalues over 2000km of Raman-amplified fiber," in *Proc. Int. Conf. Transparent Opt. Networks (ICTON)*, p. 1–4, 2018.

[24] X. Yangzhang, V. Aref, S. T. Le, H. Buelow, D. Lavery, and P. Bayvel, "Dual-polarization non-linear frequency-division multiplexed transmission with *b*-modulation," *J. Lightwave Technol.*, vol. 37, no. 6, 2019.

[25] M. Brehler, C. Mahnke, S. Chimmalgi, and S. Wahls, "NFDMLab: Simulating nonlinear frequency division multiplexing in Python," in *Proc. Opt. Fiber Commun. Conf. (OFC)*, p. 1–3, 2019.

[26] S. Wahls, S. Chimmalgi, and P. J. Prins, "FNFT: A software library for computing nonlinear Fourier transforms," *J. Open Source Softw.*, vol. 3, no. 23, p. 597, 2018.